JACS
JOURNAL OF THE AMERICAN CHEMICAL SOCIETY
pubs.acs.org/JACS
Article

Kondo Resonance of a Carbon-Centered Radical in a Single-Molecule Junction

Chengyi Chen,[#] Hua Zhu,[#] En Li, Henan Chen, Huilin Xie, Jacky W. Y. Lam, Ben Zhong Tang, Wei Ji,* and Nian Lin*

Cite This: https://doi.org/10.1021/jacs.5c09680
Read Online

ABSTRACT: The low spin−orbit coupling and weak hyperfine interactions make organic radicals promising components used in molecular spintronics. Triphenylmethyl (TPM) is the first stable carbon-centered organic radical discovered more than a century ago. Here, we use scanning tunneling spectroscopy to study quantum transport through single TPM radicals that are attached to a Au(111) electrode via atomic contacts of Ni atoms. The transport exhibits a Kondo resonance, evidencing that the unpaired electron of the radical forms a spin singlet with the itinerant electrons of the electrode. Density functional theory calculations reveal an indirect Kondo screening mechanism: the itinerant electrons couple with the radical π electron via the *d* orbitals of the Ni atoms. These results envision a new way to regulate the spin transport of organic radicals using atomic contacts in solid-state spintronic devices.

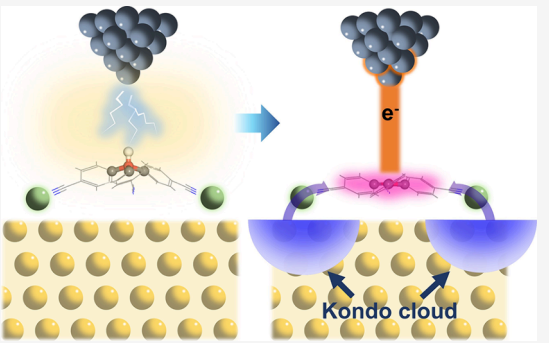

INTRODUCTION

As the prototypical carbon-centered radicals (CCRs), triphenylmethyl (TPM) radicals have been studied extensively due to their high thermal stability, kinetic persistence, and spectroscopic activity since the first isolation by Gomberg in 1900.[1] TPM radicals exhibit a narrow and intense EPR spectrum with a long spin relaxation time,[2] which is highly relevant to their applications as spin polarization agents for dynamic nuclear polarization.[3] TPM derivatives have also been used as antioxidants,[4] dopants in molecular semiconductors[5] and molecular electronics.[6,7] Furthermore, tris(4-substituted)-TPM radicals are used as building blocks for the formation of metal−organic frameworks (MOFs) comprising spin−lattices,[8] which provide a great potential of TPM to develop molecular magnetic structures with different spin topologies.[9]

The high stability and long spin relaxation time make the CCRs a promising agent for molecular spintronics.[10,11] In single-molecule spintronic devices, the spin relaxation and coherence times are further prolonged since the spins are relatively isolated with reduced spin−spin and spin−lattice interactions.[10,11] Understanding the quantum transport of CCRs at a single-molecule level is essential for designing CCR-based spintronic devices. In this regard, studying the spin transport of molecular junctions containing TPM radicals is highly relevant. Using the break-junction technique, several groups revealed that the unpaired spin in TPM radicals preserved upon interaction with metal electrodes and coherently couples to the metal electrons, forming a many-body Kondo singlet state.[12−14] These findings open the door toward CCR-based single-molecule spintronics devices.[15]

In the break-junction experiments, the detailed configuration of the molecule−metal contacts is elusive since the contacts are inaccessible or uncontrollable. It is well-known, however, that contacts play key roles in single-molecule transport. In this work, we apply scanning tunneling microscopy and spectroscopy to study the transport through single TPM radical junctions with well-defined molecule−metal contacts. Tris(4-carbonitrile)-TPM (termed TPM thereafter) coordinates with Ni atoms to form a MOF on a Au(111) surface. In this structure, each TPM is anchored by three Ni atoms on the Au(111) surface, forming single-molecule junctions of TPM-Ni_3. Spatially resolved tunneling spectroscopy at submolecule precision, complemented with density functional theory (DFT) calculations, reveals that the unpaired spin of the singly occupied molecular orbital (SOMO) of the TPM radical couples with the conduction electrons of the Au(111) substrate via the Ni atoms. The quantum transport process through the TPM radical is mediated with a Kondo singlet, which involves the conduction electrons of the Au(111) surface, the *d* orbitals of the Ni atoms, and the π orbitals of the TPM CCR. We propose that the

Received: June 9, 2025
Revised: September 4, 2025
Accepted: September 5, 2025

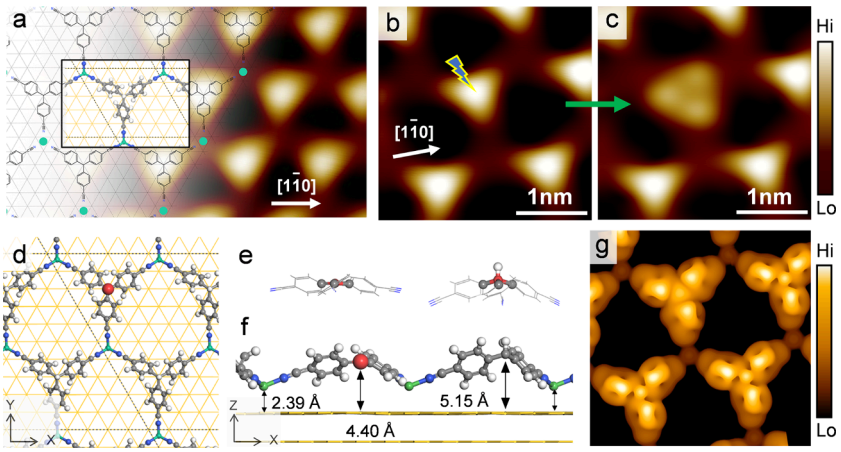

Figure 1. (a) STM image (−1 V, 50 pA) showing a 2D MOF assembled from Ni and TPM on a Au(111) substrate. (b, c) High-resolution STM images (−0.1 V, 100 pA) acquired before and after a tip manipulation at the location of the flash sign. This small bias voltage is rationally chosen to minimize the effect of electronic structure changing. (d) Fully relaxed atomic structure of a 2 × 2 Ni-TPM MOF supercell containing one d-TPM and three TPM molecules. Gray, white, blue, green, yellow, and red spheres represent C, H, N, Ni, Au, and dehydrogenated C atoms, respectively. (e) Side views of fully relaxed atomic structures of free-standing d-TPM (left panel) and TPM (right panel) molecules. (f) Side view of the fully relaxed atomic structure of the Ni-TPM MOF shown in (d). (g) Theoretically simulated constant-current STM image of the 2 × 2 MOF supercell. The bias voltage simulated is −0.1 V, and the isosurface value used to plot the isosurface contour is 2×10^{-7} e/Bohr^3. Features observed in this image are robust in varying isosurface values, as shown in the Supplementary Figure 2.

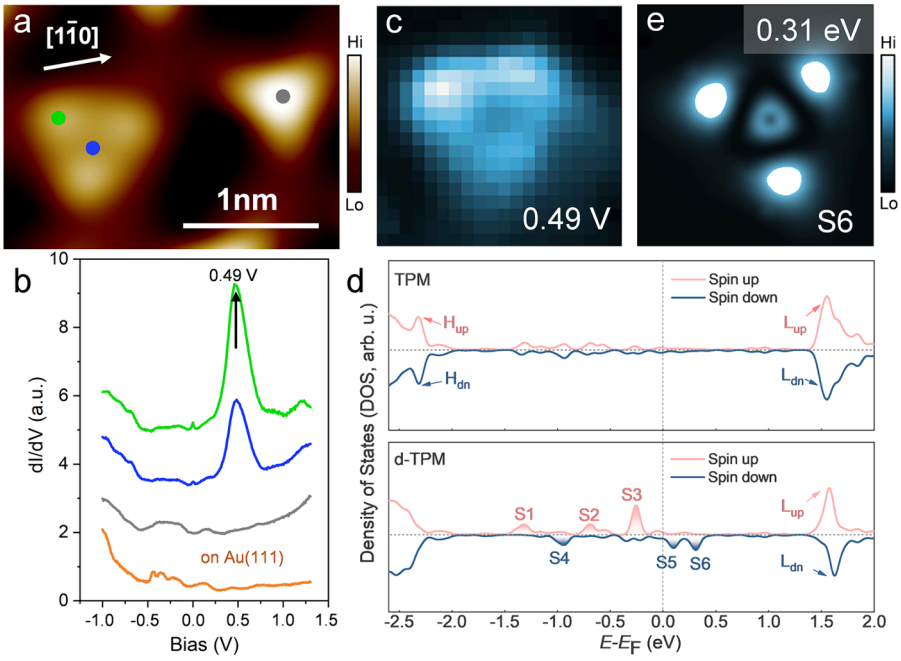

Figure 2. (a) Topographic STM (−0.1 V, 100 pA) image and (c) STS map (f = 727 Hz, I = 1000 pA, and V_{rms} = 10 mV) acquired at 0.49V for d-TPM. (b) Site-specific dI/dV spectra (f = 727 Hz, I = 1000pA, and V_{rms} = 10 mV) acquired at sites marked in (a) following the same color code. (d) Spin-polarized theoretical DOS for TPM (top panel) and d-TPM (bottom panel) molecules adsorbed on Au(111), respectively. DOS peaks corresponding to HOMO and LUMO in the up- (light red) and down-spin (dark blue) components are labeled with H_{up} and L_{up} for the up-spin and H_{dn} and L_{dn} for the down-spin. Six characteristic peaks are denoted as states S1 to S6, following the same color code of spin-up and spin-down. (e) Slab cleaved at 3.5 Å over the central carbon from the wave function norm of state S6 (0.31 eV).

quantum transport properties of TPM CCR can be tuned by replacing Ni by other transition metals with different d orbital configurations, which may open new opportunities to control the spin-dependent transport in single-molecular CCR junctions.

RESULTS AND DISCUSSION

Tris(4-carbonitrile)-TPM molecules self-assemble with Ni atoms on a Au(111) surface to form a Ni-TPM MOF. Figure 1a is an STM image showing that the TPM molecules feature a triangular cone shape, and they form a triangular lattice. The lattice vectors, 1.43 ± 0.03 nm in length, are oriented along the [01−1] directions of the Au(111) surface, matching a 5 × 5 supercell of the Au(111) atomic lattice. A large-scale STM image (Supplementary Figure 1) shows nearly defect-free large domains of the Ni-TPM MOF. A structural model of the Ni-TPM MOF is overlaid onto the STM image in Figure 1a, illustrating that each Ni atom is coordinated with three

https://doi.org/10.1021/jacs.5c09680
J. Am. Chem. Soc. XXXX, XXX, XXX−XXX

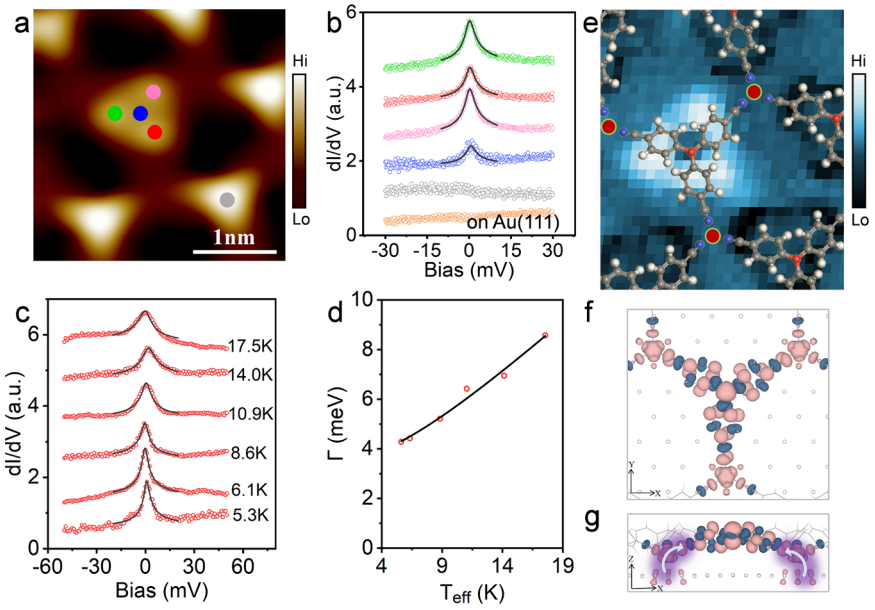

Figure 3. Kondo resonance of d-TPM. (a) STM image (−0.1 V, 100 pA) and (b) site-specific dI/dV spectra (f = 727 Hz, I = 1000 pA, and V_{rms} = 0.5 mV) acquired at the positions marked by the color dots in (a). (c) dI/dV spectra (f = 727 Hz, I = 3000 pA, and V_{rms} = 0.5 mV) measured at different temperatures. (d) Temperature dependence of Γ fitted with the Fermi-liquid model. (e) Map of ZBP intensity (f = 727 Hz, I = 3000 pA, and V_{rms} = 0.5 mV) overlaid with a Ni-TPM model. Top (f) and side (g) views of isosurface contours for the theoretical spin density distribution of d-TPM-Ni_3 adsorbed on the Au(111) substrate. The light red and dark blue colors represent spin-up and spin-down densities, respectively. The isosurface value is 4 × 10^{-4} e/Bohr^3. The white arrows in (g) illustrate the charge transfer from the substrate to the molecule.

carbonitrile (CN) ligands in a 3-fold Ni-CN_3 coordination. A DFT-optimized structural mode is plotted in the black-solid box in Figure 1a (details in Supplementary Figure 3). The central carbon atom (termed as c-C) sits at a top site of the Au(111) atomic lattice, while the Ni atoms are positioned at the hollow sites of Au(111). In the DFT-relaxed structure, the Ni−N bond exhibits a length of 1.89 Å, within the range of Ni−N coordination bonds (1.87∼2.11 Å),[16] while each Ni atom sits 2.39 Å over the Au-surface. The TPM molecules adopt a propeller conformation with three phenyl rings rotated by 52° around the C−C bonds that link the phenyls to the central carbon.

We applied an STM tip-manipulated dehydrogenation reaction to the molecule highlighted with the lightning symbol in Figure 1b, removing the hydrogen atom sitting over the central carbon atom.[17−20] This manipulation transforms the TPM into a CCR (termed d-TPM), accompanied by a topographic change from a triangular cone shape to a three-lobed triangle shape, as shown in Figure 1c. The apparent molecular height decreases from 1.84 Å (TPM) to 1.21 Å (d-TPM). We used DFT to analyze the dehydrogenated structure by constructing a 10 × 10-Au(111) supercell containing one d-TPM and three TPM molecules. Figure 1d shows the fully relaxed structure of the supercell in which the dehydrogenated c-C atom is slightly magnified and colored in red. The Ni atoms and the d-TPM molecule reside in different vertical heights, as illustrated by a side view of their atomic structure shown in Figure 1f. The dehydrogenation lowers the c-C from 5.15 to 4.40 Å above the surface. This height reduction of 0.75 Å is consistent with the apparent height change of 0.64 Å observed experimentally. In addition, the angle between the phenyl ring plane and the substrate surface decreases from 52° in TPM to 35° in d-TPM. Conformationally, d-TPM is flatter than TPM, as illustrated in the models shown in Figure 1e. These structural changes corroborate that c-C undergoes a transition from the sp^3 to sp^2 hybridization. The enhanced planarity of d-TPM can be ascribed to the p_z orbital of the c-C in the sp^2 hybridization tending to be aligned parallel with the π orbitals of the three surrounding phenyl rings. The rotation of the d-TPM observed in Figure 1c is associated with the conformational and electronic changes discussed above. The Ni atoms directly bonding to d-TPM nearly maintain their height of ∼2.39 Å above the Au(111) substrate, indicating that the dehydrogenation has minimal influence on the Ni-CN_3 coordination and Ni−Au adsorption. A simulated STM image shown in Figure 1g displays that the TPM molecules feature a central protrusion, while the d-TPM molecule features a three-lobed triangle with a lower center and slightly rotated counterclockwise with respect to the neighboring TPM molecules. The simulated image is comparable to the STM topographic images.

We applied scanning tunneling spectroscopy (STS) to probe the electronic characteristics of d-TPM. Figure 2b plots site-specific dI/dV spectra acquired at the sites indicated in Figure 2a with the same color. The spectra acquired at the TPM and at the Au(111) surface are comparable, indicating that the TPM does not possess distinctive electronic states within the measured energy range (−1.0 to 1.3 V). In contrast, d-TPM exhibits a prominent peak at 0.49 V at the three lobes of the molecule. The molecular center shows a weak peak at the same energy, which might be contributed by the states at the three neighboring lobes. Apparently, dehydrogenation introduces a new state. Figure 2c depicts an STS map acquired at 0.49, revealing that this new state spatially displays a three-lobe feature spatially.

The upper and lower panels of Figure 2d show the DFT-calculated densities of states (DOSs) of the TPM and the d-TPM molecules adsorbed on the Au(111) surface, respectively. For the TPM molecule, the highest occupied molecular orbital (HOMO) is located deeper than −2.3 eV respect to the Fermi level, and the lowest unoccupied molecular orbital (LUMO) is placed around 1.5 eV higher than the Fermi level. This over 3.8

https://doi.org/10.1021/jacs.5c09680
J. Am. Chem. Soc. XXXX, XXX, XXX−XXX

eV gap is consistent with the featureless dI/dV spectrum acquired at the TPM molecule within the range of −1.0 to 1.3 V (Figure 2b, gray). The up- and down-spin states are nearly degenerate for the adsorbed TPM molecule. However, the free-standing d-TPM radical has only one electron occupying the original HOMO of TPM, splitting the two spin components of the original HOMO. This spin-splitting leads to a spin-polarized singly occupied molecular orbital (SOMO) and a net local magnetic moment of 1.00 μ_B for the free-standing d-TPM (Supplementary Figure 4).

The spin-dependent DOS of the adsorbed d-TPM radical (lower panel of Figure 2d) shows that the SOMO and the corresponding singly unoccupied molecular orbital (SUMO) further hybridize with Ni and Au states, giving rise to multiple spin-polarized states near the Fermi level. The spin-up component (red solid line) has three major d-TPM−Ni-Au hybridized states below the Fermi level, namely S1 (peaked at −1.32 eV), S2 (peaked at −0.69 eV) and S3 (peaked at −0.27 eV). The spin-down component (blue solid line) has an occupied state S4 (peaked at −0.94 eV) and two unoccupied states S5 (peaked at 0.08 eV) and S6 (peaked at 0.31 eV). The occupation of S4, a hybridized SUMO−Ni-Au state, reduces the net magnetic moment on d-TMP from 1.00 μ_B in the free-standing form to 0.41 μ_B in the adsorbed form. Note that the direct electronic hybridization between the SOMO/SUMO of d-TPM and the d states of Ni (π-d hybridization) polarizes the Ni atoms, inducing a local magnetic moment of ∼0.51 μ_B on each Ni atom next to the d-TPM radical (Supplementary Figure 5). A DFT-simulated image of state S6 is shown in Figure 2e, whose three-lobe shape matches the state experimentally observed at 0.49 V (Figure 2c).

We next carried out tunneling spectroscopy measurements to study the quantum transport properties through d-TPM with a submolecular resolution. Figure 3b shows the site-specific dI/dV spectra acquired at the three lobes (color in green, red, and pink) and the center of a d-TPM radical (color in blue), as marked with the colored dots in Figure 3a. Every spectrum acquired on d-TPM displays a distinct zero bias peak (ZBP). This feature is absent in spectra acquired on the TPM (gray curve) or Au(111) (orange curve). The ZBPs in these dI/dV spectra can be fitted using a Fano-Frota line shape,[21,22] revealing a half-width at half-maximum (Γ) of 4.3 ± 0.3 meV, we also fitted them using a Fano line shape as a reference (details in Supplementary Figures 6). We acquired temperature-dependent spectra, as plotted in Figure 3c. Figure 3d shows the temperature-dependent peak width (Γ) of the ZBPs. A Kondo temperature T_K of 40.8 ± 2.6 K and an empirical parameter α = 10.3 ± 0.3 are derived by fitting these data using the equation of the Fermi-liquid model (the detail of the fitting is shown in Supplementary Note 1). Given the presence of local magnetic moments and the temperature-dependent peak broadening, we, therefore, attribute the ZBP to a Kondo resonance originated from the many-body Kondo singlet state comprising the residual local magnetic moment of the d-TPM radical and the itinerant electrons of the Au(111) substrate.[17,23−35]

Figure 3e shows the dI/dV mapping of ZBP intensity, representing the spatial distribution of the Kondo cloud. The observed high-intensity area displays a three-lobe feature with the ZBP signal at the three phenyl rings being stronger than that at the c-C. A careful inspection reveals that the ZBP intensity maxima are located at the side C—C bonds of the phenyl rings. A DFT-calculated spin density map of d-TPM shown in Figure 3f,g, however, reveals that c-C has the largest spin density (local magnetic moment of 0.17 μ_B), while the spin density at each phenyl-carbonitrile arm is smaller (integrated local magnetic moment of 0.08 μ_B). (Supplementary Figure 5). In most previous studies of π-radical Kondo resonance, the Kondo clouds were found to spatially coincide with the corresponding spin density distributions of the SOMO or SUMO.[36−40] Here, our observation that the Kondo cloud does not match the spin density distribution suggests different Kondo screening mechanisms.

At a temperature below the Kondo temperature, conduction electrons from the Au substrate are prone to screen the local magnetic moments by introducing a state of the minority spin at the Fermi level, forming a Kondo singlet with the local magnetic moment. As shown in the spin density map (Figure 3f), spin-up is the majority spin, and the local magnetic moment is primarily contributed by the d-TPM radical and the three neighboring Ni atoms. The magnetic moments on Ni atoms can be directly screened by spin-down electrons of the Au substrate through overlap of wave functions. However, as revealed in the side view of the spin density (Figure 3g), the d-TPM radical interacts with the Au(111) substrate through three coordinating Ni atoms, forming a d-TPM-Ni_3 molecular junction. At this junction, the molecular backbone of the d-TPM radical, including the c-C atom and three phenyl rings, is essentially isolated from the substrate. As a result, direct screening of the π-radical local magnetic moment by the substrate electrons is suppressed due to the large spatial separation. As an alternative, indirect screening through three Ni atoms plays a significant role in screening the π-radical local magnetic moment of d-TPM.

To elucidate the indirect screening mechanism, we analyze the hybridization among the projected density of states of d-TPM π states, Ni d states, and the Au substrate states (Figure 4a), whereas Figure 4b shows the wave functions of states S1 to S6 (first marked in Figure 2d) exhibiting the SOMO or SUMO-like character. Figure 4a shows that states S1, S3, and S6 hybridize negligibly with the Au substrate states. This conclusion is further corroborated by their real-space wave function norm maps, depicted in Figure 4b, which reveal

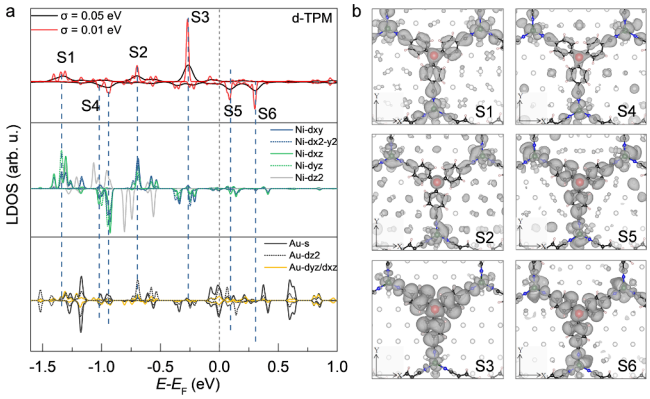

Figure 4. Hybridization between the molecular orbitals of d-TPM, Ni d orbitals, and Au substrate states. (a) Spin-polarized, atom and orbital decomposed local density of states (LDOS) of the whole d-TPM molecule (top panel), of its nearest-neighbor Ni atom (middle panel), and of the Au atom below the Ni atom (bottom panel). Variable σ in the top panel specifies the width of electronic smearing used in plotting the curves. Six states S1 to S6 are marked in the top panel. Three horizontal dashed lines separate the spin-up and spin-down curves. (b) Top view of isosurface contours for the wave function norms of states S1−S6. The isosurface value is 5 × 10^{-5} e/Bohr^3.

https://doi.org/10.1021/jacs.5c09680
J. Am. Chem. Soc. XXXX, XXX, XXX−XXX

minimal substrate contributions to these states. Thus, we argue that electron tunnelling probability through states S1, S3, or S6 is significantly suppressed. In contrast, states S2, S4, and S5 form hybridized states that combine the SOMO or SUMO, the Ni d-states, and the Au substrate states. Figure 4b confirms the Au-derived contributions to their wave function norm maps. Therefore, these three states dominate charge transport through the d-TPM-Ni_3 junction. Interestingly, the two occupied states S2 and S4 exhibit appreciable charge densities distributed around the edges of the three phenyl rings, coinciding with the observed ZBP intensity maxima located at the edges of the phenyl rings.

Notably, state S5 is particularly interesting because it resides only 0.08 eV from the Fermi level at the Γ point. This state is dispersive across the Brillouin zone, exhibiting a partially occupied band (Supplementary Figure 7), which is pinned around the Fermi level by the surface states of the Au substrate. Therefore, once the Kondo resonance emerges in the spin-down component, these spin-down conduction electrons from the Au substrate can readily populate state S5 through the Ni bridging, injecting additional spin-down electrons into the molecular backbone and thereby further quenching the local magnetic moment on d-TPM. Moreover, a complementary screening route may also work in which spin-down electrons accumulate in Au surface states directly beneath the d-TPM-Ni_3 complex, forming a magnetic dipole.

CONCLUSION

In summary, we have studied the quantum transport properties through a neutral CCR molecule in a single-molecule junction. We demonstrate that the local magnetic moment of the CCR is mostly preserved in the junction, as evidenced by the presence of a fully screened spin-1/2 Kondo resonance. Substantiated with DFT analysis, we attribute the formation of the Kondo singlet to multiple mechanisms, including direct screening by the Au substrate and indirect screening via the Ni atomic contacts and magnetic dipoles. The findings reported here open an avenue toward regulating spin-dependent transport through organic radicals by the choice of specific atomic contacts. Furthermore, the stability of the neutral CCR makes these radicals an excellent platform for studying Kondo physics of complex structures such as Kondo lattice.[41,42]

EXPERIMENTAL METHODS

Sample Preparation and Measurement. All the synthesis and measurements are carried out under an ultrahigh vacuum environment (base pressure $<5.0 \times 10^{-10}$ mbar) equipped with a CreaTec low-temperature STM. A single-crystalline Au(111) substrate was cleaned via repeated Ar^+ sputtering and annealing cycles. Tris(4-carbonitrile)-TPM molecules were sublimated from a Knudsen cell at 155 °C and deposited onto the Au(111) substrate. Ni atoms were evaporated using direct current heating. After deposition, the sample was annealed at 135 °C for 15 min. All the STM and STS data were acquired at 5.3 K. Differential conductance spectra were acquired using the lock-in technique with a root-mean-square (rms) amplitude of 0.5 mV. As a reference, the *I*-*V* curves of the differential conductance spectra are numerically derivatized to obtain the absolute value conductance referring to zero conductance (Supplementary Figure 8).

Tip Manipulation. The tip was moved above the center of the TPM molecule. Then, the bias and tunnel current were set as $V = 3.5$ V, $I = 300$ pA, and the bias was gradually increased to 4.0 V until the current reading suddenly dropped.

DFT Calculations. DFT calculations were performed using the generalized gradient approximation for the exchange-correlation potential, the projector augmented wave method,[43,44] and a plane wave basis set, as implemented in the Vienna ab initio simulation package (VASP).[45] van der Waals interactions were considered at the DFT-D3 level for all calculations, using the Perdew−Burke−Ernzerhof (PBE) functional.[46] The kinetic energy cutoff for the plane-wave basis was set to 400 eV, and a vacuum layer of around 16 Å was adopted to model the TPM-Ni/Au(111) system in all calculations. For the TPM-Ni/5 × 5-Au(111) supercell, a *k*-mesh of 3 × 3 × 1 was used for both geometric optimization and electronic structure calculations. For the TPM-Ni/10 × 10-Au(111) supercell, due to the larger size of the system, a *k*-mesh of 1 × 1 × 1 was adopted for geometric optimization and electronic structure calculations. During the structural relaxation process, the bottom three layers of Au atoms were fixed, and the surface Au and molecules were relaxed until the residual force on each atom was less than 0.05 eV/Å. Our STM image simulations were carried out using the Tersoff-Hamann (T-H) approximation. The core formula is

$$I \propto \sum_{v} |\psi_v(\vec{r_0})|^2 \delta(E_v - E_F)$$

in which, I represents the tunneling current, $\psi_v(\vec{r_0})$ denotes the wave functions of the sample at the tip position (r_0).[47]

ASSOCIATED CONTENT

Supporting Information

The Supporting Information is available free of charge at https://pubs.acs.org/doi/10.1021/jacs.5c09680.

Large-scale STM topography of the Ni-TPM MOF; DFT-simulated STM images; DFT-optimized atomic structure of TPM-Ni MOF/Au(111); Gas-phase calculated molecular conformation; frontier molecular orbitals and spin density of TPM and d-TPM; projected magnetic moment on the d-TPM; dI/dV spectra fitted using a Fano-Frota line shape and a Fano line shape; DFT-calculated spin-down projected band structure of the d-TPM molecule; numerical derivative of the I−V spectra; and the Kondo temperature fitting procedure (PDF)

AUTHOR INFORMATION

Corresponding Authors

Wei Ji − *Beijing Key Laboratory of Optoelectronic Functional Materials & Micro-Nano Devices, School of Physics, Renmin University of China, Beijing 100872, China;* orcid.org/0000-0001-5249-6624; Email: wji@ruc.edu.cn

Nian Lin − *Department of Physics, The Hong Kong University of Science and Technology, Hong Kong 999077, China;* orcid.org/0000-0001-5693-4011; Email: phnlin@ust.hk

Authors

Chengyi Chen − *College of Mechanical and Electrical Engineering, Fujian Agriculture and Forestry University, Fuzhou, Fujian 350002, China; Department of Physics, The Hong Kong University of Science and Technology, Hong Kong 999077, China;* orcid.org/0000-0001-9216-0551

Hua Zhu − *Beijing Key Laboratory of Optoelectronic Functional Materials & Micro-Nano Devices, School of Physics, Renmin University of China, Beijing 100872, China*

En Li − *Department of Physics, The Hong Kong University of Science and Technology, Hong Kong 999077, China*

Henan Chen − *Department of Physics, The Hong Kong University of Science and Technology, Hong Kong 999077, China*

Huilin Xie − *School of Science and Engineering, Guangdong Basic Research Center of Excellence for Aggregate Science, Shenzhen Institute of Aggregate Science and Technology, The*

https://doi.org/10.1021/jacs.5c09680
J. Am. Chem. Soc. XXXX, XXX, XXX−XXX

Chinese University of Hong Kong, Shenzhen (CUHK-Shenzhen), Shenzhen, Guangdong 518172, China

Jacky W. Y. Lam − *Department of Chemistry, and the Hong Kong Branch of Chinese National Engineering Research Center for Tissue Restoration and Reconstruction, The Hong Kong University of Science and Technology, Hong Kong 999077, China*

Ben Zhong Tang − *School of Science and Engineering, Guangdong Basic Research Center of Excellence for Aggregate Science, Shenzhen Institute of Aggregate Science and Technology, The Chinese University of Hong Kong, Shenzhen (CUHK-Shenzhen), Shenzhen, Guangdong 518172, China; Department of Chemistry, and the Hong Kong Branch of Chinese National Engineering Research Center for Tissue Restoration and Reconstruction, The Hong Kong University of Science and Technology, Hong Kong 999077, China;* orcid.org/0000-0002-0293-964X

Complete contact information is available at: https://pubs.acs.org/10.1021/jacs.5c09680

Author Contributions

#C.C. and H.Z. contributed equally to this work. The manuscript was written through contributions of all authors. All authors have given approval to the final version of the manuscript.

Notes

The authors declare no competing financial interest.

■ ACKNOWLEDGMENTS

This work is financially supported by the Hong Kong RGC (project 16301423), the National Natural Science Foundation of China (Grants No. 92477205 and No. 52461160327), the National Key R&D Program of China (Grant No. 2023YFA1406500), the Physics Lab of High-Performance Computing (PLHPC), the Public Computing Cloud (PCC) of Renmin University of China, and the Innovation and Technology Commission of Hong Kong (ITC−CNERC14SC01).

■ REFERENCES

(1) Gomberg, M. An instance of trivalent carbon: Triphenylmethyl. *J. Am. Chem. Soc.* **1900**, *22* (11), 757−771.

(2) Weissman, S.; Feher, G.; Gere, E. The Spin Relaxation Time of Triphenylmethyl at Low TEMPERATURES1. *J. Am. Chem. Soc.* **1957**, *79* (20), 5584−5585.

(3) Biedenbänder, T.; Aladin, V.; Saeidpour, S.; Corzilius, B. R. Dynamic nuclear polarization for sensitivity enhancement in biomolecular solid-state NMR. *Chem. Rev.* **2022**, *122* (10), 9738−9794.

(4) Jiménez, A.; Selga, A.; Torres, J. L.; Julià, L. Reducing activity of polyphenols with stable radicals of the TTM series. Electron transfer versus H-abstraction reactions in flavan-3-ols. *Org. Lett.* **2004**, *6* (24), 4583−4586.

(5) Porter, W. W.; Vaid, T. P. Doping of an organic molecular semiconductor by substitutional cocrystallization with a molecular n-dopant. *J. Mater. Chem.* **2007**, *17* (5), 469−475.

(6) Hicks, R. *Stable radicals: fundamentals and applied aspects of odd-electron compounds*; John Wiley & Sons, 2011.

(7) Ji, L.; Shi, J.; Wei, J.; Yu, T.; Huang, W. Air-Stable Organic Radicals: New-Generation Materials for Flexible Electronics? *Adv. Mater.* **2020**, *32* (32), No. 1908015.

(8) Heuer, A. M.; Coste, S. C.; Singh, G.; Mercado, B. Q.; Mayer, J. M. A Guide to Tris (4-Substituted)-triphenylmethyl Radicals. *J. Org. Chem.* **2023**, *88* (14), 9893−9901.

(9) Kimura, S.; Uejima, M.; Ota, W.; Sato, T.; Kusaka, S.; Matsuda, R.; Nishihara, H.; Kusamoto, T. An open-shell, luminescent, two-dimensional coordination polymer with a honeycomb lattice and triangular organic radical. *J. Am. Chem. Soc.* **2021**, *143* (11), 4329−4338.

(10) Sanvito, S. Molecular spintronics. *Chem. Soc. Rev.* **2011**, *40* (6), 3336−3355.

(11) Yeo, H.; Debnath, S.; Krishnan, B. P.; Boudouris, B. W. Radical polymers in optoelectronic and spintronic applications. *RSC Appl. Polym.* **2024**, *2* (1), 7−25.

(12) Appelt, W. H.; Droghetti, A.; Chioncel, L.; Radonjić, M.; Muñoz, E.; Kirchner, S.; Vollhardt, D.; Rungger, I. Predicting the conductance of strongly correlated molecules: the Kondo effect in perchlorotriphenylmethyl/Au junctions. *Nanoscale* **2018**, *10* (37), 17738−17750.

(13) Frisenda, R.; Gaudenzi, R.; Franco, C.; Mas-Torrent, M.; Rovira, C.; Veciana, J.; Alcon, I.; Bromley, S. T.; Burzurí, E.; Van der Zant, H. S. Kondo effect in a neutral and stable all organic radical single molecule break junction. *Nano Lett.* **2015**, *15* (5), 3109−3114.

(14) Mitra, G.; Low, J. Z.; Wei, S.; Francisco, K. R.; Deffner, M.; Herrmann, C.; Campos, L. M.; Scheer, E. Interplay between magnetoresistance and kondo resonance in radical single-molecule junctions. *Nano Lett.* **2022**, *22* (14), 5773−5779.

(15) Li, L.; Prindle, C. R.; Shi, W.; Nuckolls, C.; Venkataraman, L. Radical single-molecule junctions. *J. Am. Chem. Soc.* **2023**, *145* (33), 18182−18204.

(16) Peskov, M. V.; Schwingenschlögl, U. Photophysical properties of open-framework germanates templated by nickel complexes. *Phys. Chem. Chem. Phys.* **2014**, *16* (22), 10891−10896.

(17) Zhao, A.; Li, Q.; Chen, L.; Xiang, H.; Wang, W.; Pan, S.; Wang, B.; Xiao, X.; Yang, J.; Hou, J. Controlling the Kondo effect of an adsorbed magnetic ion through its chemical bonding. *Science* **2005**, *309* (5740), 1542−1544.

(18) Liu, L.; Yang, K.; Jiang, Y.; Song, B.; Xiao, W.; Li, L.; Zhou, H.; Wang, Y.; Du, S.; Ouyang, M. Reversible single spin control of individual magnetic molecule by hydrogen atom adsorption. *Sci. Rep.* **2013**, *3* (1), 1210.

(19) Karan, S.; Li, N.; Zhang, Y.; He, Y.; Hong, I. P.; Song, H.; Lü, J. T.; Wang, Y.; Peng, L.; Wu, K.; Michelitsch, G. S.; Maurer, R. J.; Diller, K.; Reuter, K.; Weismann, A.; Berndt, R. Spin manipulation by creation of single-molecule radical cations. *Phys. Rev. Lett.* **2016**, *116* (2), No. 027201.

(20) Li, R.; Li, N.; Wang, H.; Weismann, A.; Zhang, Y.; Hou, S.; Wu, K.; Wang, Y. Tuning the spin-related transport properties of FePc on Au (111) through single-molecule chemistry. *Chem. Commun.* **2018**, *54* (66), 9135−9138.

(21) Frota, H. Shape of the Kondo resonance. *Phys. Rev. B* **1992**, *45* (3), 1096.

(22) Frank, S.; Jacob, D. Orbital signatures of Fano-Kondo line shapes in STM adatom spectroscopy. *Phys. Rev. B* **2015**, *92* (23), No. 235127.

(23) Knorr, N.; Schneider, M. A.; Diekhöner, L.; Wahl, P.; Kern, K. Kondo effect of single Co adatoms on Cu surfaces. *Phys. Rev. Lett.* **2002**, *88* (9), No. 096804.

(24) Manoharan, H.; Lutz, C.; Eigler, D. Quantum mirages formed by coherent projection of electronic structure. *Nature* **2000**, *403* (6769), 512−515.

(25) Madhavan, V.; Chen, W.; Jamneala, T.; Crommie, M.; Wingreen, N. Tunneling into a single magnetic atom: spectroscopic evidence of the Kondo resonance. *Science* **1998**, *280* (5363), 567−569.

(26) Li, J.; Schneider, W.-D.; Berndt, R.; Delley, B. Kondo scattering observed at a single magnetic impurity. *Phys. Rev. Lett.* **1998**, *80* (13), 2893.

(27) Néel, N.; Kröger, J.; Limot, L.; Palotas, K.; Hofer, W.; Berndt, R. Conductance and Kondo effect in a controlled single-atom contact. *Phys. Rev. Lett.* **2007**, *98* (1), No. 016801.

(28) Ternes, M.; Heinrich, A. J.; Schneider, W.-D. Spectroscopic manifestations of the Kondo effect on single adatoms. *J. Phys.: Condens.Matter* **2009**, *21* (5), No. 053001.

(29) Iancu, V.; Deshpande, A.; Hla, S.-W. Manipulation of the Kondo effect via two-dimensional molecular assembly. *Phys. Rev. Lett.* **2006**, *97* (26), No. 266603.

(30) Komeda, T.; Isshiki, H.; Liu, J.; Zhang, Y.-F.; Lorente, N.; Katoh, K.; Breedlove, B. K.; Yamashita, M. Observation and electric current control of a local spin in a single-molecule magnet. *Nat. Commun.* **2011**, *2* (1), 217.
(31) Chen, W.; Yan, Y.; Ren, M.; Zhang, T.; Feng, D. Two-impurity Kondo effect in potassium-doped single-layer p-sexiphenyl films. *Sci. China: Phys., Mech. Astron.* **2022**, *65* (4), 246811.
(32) Jarillo-Herrero, P.; Kong, J.; Van Der Zant, H. S.; Dekker, C.; Kouwenhoven, L. P.; De Franceschi, S. Orbital Kondo effect in carbon nanotubes. *Nature* **2005**, *434* (7032), 484−488.
(33) Wahl, P.; Diekhöner, L.; Wittich, G.; Vitali, L.; Schneider, M.; Kern, K. Kondo effect of molecular complexes at surfaces: Ligand control of the local spin coupling. *Phys. Rev. Lett.* **2005**, *95* (16), No. 166601.
(34) Fernández-Torrente, I.; Franke, K.; Pascual, J. Vibrational Kondo effect in pure organic charge-transfer assemblies. *Phys. Rev. Lett.* **2008**, *101* (21), No. 217203.
(35) Tsukahara, N.; Shiraki, S.; Itou, S.; Ohta, N.; Takagi, N.; Kawai, M. Evolution of Kondo resonance from a single impurity molecule to the two-dimensional lattice. *Phys. Rev. Lett.* **2011**, *106* (18), No. 187201.
(36) Patera, L. L.; Sokolov, S.; Low, J. Z.; Campos, L. M.; Venkataraman, L.; Repp, J. Resolving the Unpaired-Electron Orbital Distribution in a Stable Organic Radical by Kondo Resonance Mapping. *Angew. Chem., Int. Ed.* **2019**, *58* (32), 11063−11067.
(37) Turco, E.; Bernhardt, A.; Krane, N.; Valenta, L.; Fasel, R.; Juríček, M.; Ruffieux, P. Observation of the magnetic ground state of the two smallest triangular nanographenes. *JACS Au* **2023**, *3* (5), 1358−1364.
(38) Sun, Q.; Mateo, L. M.; Robles, R.; Lorente, N.; Ruffieux, P.; Bottari, G.; Torres, T.; Fasel, R. Bottom-up Fabrication and Atomic-Scale Characterization of Triply Linked, Laterally π-Extended Porphyrin Nanotapes. *Angew. Chem.* **2021**, *133* (29), 16344−16350.
(39) Vilas-Varela, M.; Romero-Lara, F.; Vegliante, A.; Calupitan, J. P.; Martínez, A.; Meyer, L.; Uriarte-Amiano, U.; Friedrich, N.; Wang, D.; Schulz, F.; Koval, N. E.; Sandoval-Salinas, M. E.; Casanova, D.; Corso, M.; Artacho, E.; Peña, D.; Pascual, J. I. On-Surface Synthesis and Characterization of a High-Spin Aza-[5]-Triangulene. *Angew. Chem., Int. Ed.* **2023**, *62* (41), No. e202307884.
(40) Calvo-Fernández, A.; Kumar, M.; Soler-Polo, D.; Eiguren, A.; Blanco-Rey, M.; Jelínek, P. Theoretical model for multiorbital Kondo screening in strongly correlated molecules with several unpaired electrons. *Phys. Rev. B* **2024**, *110* (16), No. 165113.
(41) Si, Q.; Smith, J. L.; Ingersent, K. Quantum critical behavior in Kondo systems. *Int. J. Mod. Phys. B* **1999**, *13* (18), 2331−2342.
(42) Doniach, S. The Kondo lattice and weak antiferromagnetism. *Phys. B+C* **1977**, *91*, 231−234.
(43) Kresse, G.; Joubert, D. From ultrasoft pseudopotentials to the projector augmented-wave method. *Phys. Rev. B* **1999**, *59* (3), 1758.
(44) Blöchl, P. E. Projector augmented-wave method. *Phys. Rev. B* **1994**, *50* (24), 17953.
(45) Kresse, G.; Furthmüller, J. Efficient iterative schemes for ab initio total-energy calculations using a plane-wave basis set. *Phys. Rev. B* **1996**, *54* (16), 11169.
(46) Perdew, J. P.; Burke, K.; Ernzerhof, M. Generalized gradient approximation made simple. *Phys. Rev. Lett.* **1996**, *77* (18), 3865.
(47) Tersoff, J.; Hamann, D. R. Theory of the scanning tunneling microscope. *Phys. Rev. B* **1985**, *31* (2), 805.

https://doi.org/10.1021/jacs.5c09680
J. Am. Chem. Soc. XXXX, XXX, XXX−XXX